

# Electrodynamics of the Planar Negative Index Lens

Nicholas A. Kuhta

Research Advisor: Viktor A. Podolskiy

06/15/2007

## **Abstract**

We analyze a planar lens with negative index of refraction to develop analytical expressions describing EM evanescent and propagating waves. Resolution, field magnitude, and field intensity of the superlens is identical for equal absorption and gain parameters. Subwavelength resolution is achieved by the Planar NIM lens in the near-field regime due to amplification and recovery of evanescent field components. A delta source Green's function and exact transfer functions for the system were used to define the transition to diffraction limited imaging behavior as a function of system absorption and size. Far-field analysis was performed by calculating fields using a Fresnel integral to show asymmetric field confinement and diffraction limited resolution.

## **Introduction**

Optical imaging provides important physical information about objects and their surroundings. Geometrical optics images objects by focusing light from a source through lenses, after which light meets back at a pre-determined location to make an image. Unfortunately, geometrical optics is limited by the inherent properties of light. When a plane wave goes through a slit the waves spread out in a spherical pattern. Huygens principle explains this phenomenon by stating that light waves are comprised of individual spherical waves existing at the crests of planar wavefronts. The spreading out of light is referred to as diffraction. Due to the diffractive nature of light, geometrical optics has a fundamental limit, called the diffraction limit, which states that one can only image an object that has feature sizes on the order of the wavelength of source light used to illuminate it.

In the future it could be possible to image single protein molecules with visible light using technology that outperforms diffraction limited imaging systems. Hopefully a collaborative effort will help scientists find materials that allow us to physically see molecular behavior. The index of refraction is a measure of material response to external electric and magnetic fields.

$$n = \pm\sqrt{\epsilon\mu} \quad (1)$$

Conventional optical materials have a positive index of refraction, but the square root in Eq (1) shows that  $n$  values could be either positive or negative. If both  $\epsilon$  and  $\mu$  are simultaneously negative, then a negative index of refraction (NIM) is the correct physical assignment. [1] Thus far researchers at UC Berkeley and Maryland can resolve objects that are  $200nm$  in size [2, 3], and hopefully future endeavors into the development of NIM technology will generate new physics.

Compactness, and extreme increases in speed are important new reasons why optics should be used to move modern technology forward. Optical computing may soon be realized as photon transmission can be switched on and off using all-optical transistors in a non-linear photonic crystal. [4] Considerable effort is being put forth to find new optical materials and waveguide structures that allow scientists to control the storage and transmission of light. Negative index of refraction materials top the list, as they enable subwavelength field confinement which could be used for data storage and near-field microscopy applications.

The phase velocity of EM waves moving in negative index material opposes the propagation direction while the energy moves in the propagation direction. Interesting NIM electrodynamic properties resulting from negative phase velocity are: a reversed doppler shift, inverse Snell's law, and optically perfect lenses. In particular, inverse Snell's law is shown when NIM systems bend light so the refraction occurs on the same side of the surface normal as the incident source. [1, 5] So far NIM technology has enabled researchers to image with  $60\text{ nm}$  half pitch resolution, which was one sixth of the illumination wavelength. [6]

The elusiveness of NIM is due to no known naturally occurring isotropic materials having simultaneously negative  $\epsilon$  and  $\mu$  at the same frequency. Metamaterials derive their properties from physical structure instead of composition, and are commonly used for NIM devices. There have been experimental observations of negative refraction at  $10.5\text{ GHz}$  in metamaterials. [7] Negative permittivity and induced magnetic resonance have been used in arrays of metallic split rings to achieve negative refraction at  $100\text{ THz}$ . [8] Structures containing metal-dielectric layers and split ring resonators have been engineered to achieve negative  $\epsilon$  and  $\mu$  at microwave,

near-infrared, and visible frequencies. [9, 10]

The superlens is a planar lens with index of refraction  $n \simeq -1$ , where  $\epsilon = -1 \pm i\epsilon''$ , and  $\mu = -1 \pm i\mu''$ . Work describing the dielectric constant in tensor form will be presented elsewhere. The imaginary part of the permittivity and permeability terms represent the absorption or gain of the system. Many research groups have shown that the near-field superlens resolution outperforms the diffraction limit, while the far-field system region has resolution limitations. [1, 5, 6, 7, 11, 16, 19]

The first purpose of this work is to discuss the geometry of the superlens system in the near-field regime and describe the resolution. Our near-field models are constructed from a single slit model using a transfer function method which is derived from transmission and reflection coefficients. The next topic of discussion will be the transition to far-field behavior for the system by imaging a point source as the size of the system becomes larger. We will describe the critical lens thickness as a function of absorption where the evanescent waves become smaller than the propagating waves. Finally, we will solve a Fresnel integral for a point source to show that there is asymmetric field confinement at the image location when the system is in the far-field regime resulting in loss of subwavelength resolution capabilities.

One interesting aspect of our work that we have yet to explore is applications for controlled directional flow of surface plasmons at the lens boundaries. Our time-domain animations show surface plasmons exist at each lens boundary when the system is in the near-field regime. The direction of these waves can be controlled by introducing a source into the system. One interesting approach entails optimizing the system for surface plasmon formation to see whether or not coupling to the system could create a new optical switching device.

### Near-Field Single Slit (NIM) Imaging

All of our models describe TM Polarized electromagnetic field solutions obtained by the summation of field terms in wavevector space. For the single slit the source term is derived from a fourier integral over the width of the slit. By defining the width of the slit as  $w$ , the source equation or *wavevector spectrum* for the single slit can be calculated as shown below.

$$a(k_x) = \int_{-w/2}^{w/2} e^{ik_x x} = 2 \frac{\sin(w \cdot k_x/2)}{k_x} \quad (2)$$

We use Maxwell's equations with dielectric boundary conditions to solve for reflection and transmission coefficients. To calculate field solution we first separate the system into three regions. The first region is before the lens, the second inside the lens, and the third behind the lens. Requiring the surface parallel components of the  $\vec{E}$  and  $\vec{H}$  fields to be continuous across each lens boundary provides enough information to solve for the four reflection and transmission coefficients. By using the *wavevector spectrum* shown above we can write field solutions in each region as summations in k-space.

$$\vec{H}_1 = \sum_{k_x} a(k_x) [\exp[i(k_{z_1} z + k_x x - \omega t)] + r_1 \exp[i(-k_{z_1} z + k_x x - \omega t)]] \quad (3)$$

$$\vec{H}_2 = \sum_{k_x} a(k_x) [t_2 \exp[i(k_{z_2} z + k_x x - \omega t)] + r_2 \exp[i(-k_{z_2} z + k_x x - \omega t)]] \quad (4)$$

$$\vec{H}_3 = \sum_{k_x} a(k_x) [t_3 \exp[i(k_{z_1} z + k_x x - \omega t)]] \quad (5)$$

The planar lens focal distance is defined as the length between the source and the front lens interface. In our simulations we label the focal distance with the variable  $a$ . The lens thickness of the system is labelled  $b$ . Geometric optics shows that the image location for the planar NIM lens is at a distance  $(b - a)$  behind the lens. For a real image to exist, the lens thickness must be greater than or equal to the focal distance. We use TM polarized light sources for all models presented in this work. By using the dispersion relationship,

$$k^2 = n^2 \frac{\omega^2}{c^2} \quad (6)$$

the propagation wave vector can be given by the expression

$$k_z = \sqrt{\frac{n^2 \omega^2}{c^2} - k_x^2} \quad (7)$$

The resolution limit in optics is caused by diffraction, or the spreading out of waves. As seen

from equation 7, once  $k_x^2$  becomes greater than  $n^2\omega^2/c^2$ , the propagating wavevector becomes complex. Imaginary  $k_z$  values correspond to *evanescent* waves that exponentially decay away from a source. In order to image small features one must use large  $k_x$  values due to the fact that  $k_x$  is inversely proportional to wavelength. Therefore, the resolution limit in conventional optics is proportional to the wavelength of the source. One way to overcome the diffraction limit is to position a microscope in the near-field in order to measure the evanescent waves before they have decayed beyond detection. The resolution of near-field microscopes is on the order of  $\Delta \approx 2a$ . [12]

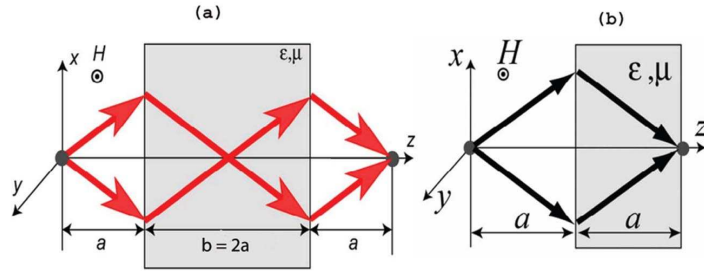


Figure 1: General Ray Diagram for the Planar NIM Superlens. a) Image locate is at a distance  $(b - a)$  behind the lens. When  $b = 2a$  the system is in the *symmetric* configuration. b) When  $a = b$  the image is located at the back lens interface. This is the *optimal* lens configuration.

Spacial field expressions can be written as a linear combination of plane waves as shown in Eqs(3, 4, 5). It is equivalent to calculate analytical field solutions in k-space using the wavevector spectrum  $a(k_x)$  to represent the source information, and a transfer function  $\tau(x, z, \omega, k_x)$  to account for the imaging system contribution. [11, 13, 14, 15]

$$H_y(x, z, t) = \int a(k_x)\tau(x, z, \omega, k_x)e^{-i\omega t}dk_x \quad (8)$$

Between the source and the front lens interface, the transfer function describing the  $y$  component of the H-Field is shown in Eq (9). This transfer function accounts for incident, reflected, and scattered field components. For TM waves, the transfer-in function represents the  $y$  component of the H-field inside the superlens system by including transmission and reflection information. Likewise, a transfer-out function describes the  $y$  component of the H-field after the back lens interface. [16] All transfer functions shown below represent series solutions of exact equations

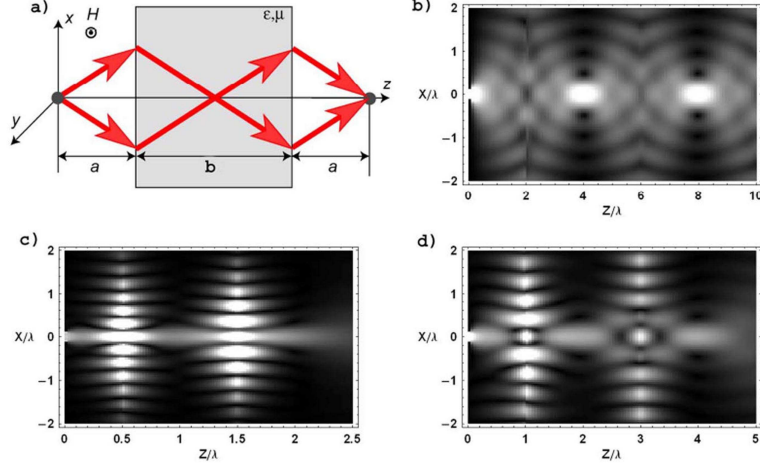


Figure 2: a) Planar NIM lens ray diagram where the focal distance is  $a$ , and the lens thickness is  $b = 2a$ . The image location is at a distance of  $(b - a)$  behind the lens. To create an image  $a \leq b$ . The grey region represents the planar NIM superlens. b) H-Field intensity plot for slit width  $= 0.25\lambda$ , focal distance  $a = 2.0\lambda$ , lens thickness  $b = 4.0\lambda$ , image location  $= 8.0\lambda$ . c) H-Field intensity plot for slit width  $= 0.25\lambda$ , focal distance  $a = 0.5\lambda$ , lens thickness  $b = 1.0\lambda$ , image location  $= 2.0\lambda$ . d) H-Field intensity plot for slit width  $= 0.25\lambda$ , focal distance  $a = 1.0\lambda$ , lens thickness  $b = 2.0\lambda$ , image location  $= 4.0\lambda$ . The gain and absorption parameters for all of these field intensity plots are  $\epsilon'' = \mu'' = \pm 10^{-3}$ .

calculated in the limit of small gain and absorption.

$$\tau_{before}(x, z, k_x, \omega) = e^{-\kappa_z + ik_x x} + \frac{i\phi e^{\kappa_z(2b-2a+z)}}{1 + \phi^2 e^{2\kappa_z b}} e^{ik_x x} \quad (9)$$

$$\tau_{in}(x, z, k_x, \omega) = \frac{e^{\kappa_z(z-2a)} + i\phi e^{\kappa_z(2b-z)}}{(1 + i\phi)(1 + \phi^2 e^{2\kappa_z b})} e^{ik_x x} \quad (10)$$

$$\tau_{out}(x, z, k_x, \omega) = \frac{e^{\kappa_z(2b-z)}}{1 + \phi^2 e^{2\kappa_z b}} e^{ik_x x} \quad (11)$$

where  $\kappa_z = \sqrt{k_x^2 - \omega^2/c^2}$ , and the parameter

$$\phi = \frac{1}{2} \left[ \epsilon'' + \frac{\epsilon'' + \mu''}{2(k_x^2 c^2/\omega^2 - 1)} \right], \text{ where } |\phi| \ll 1. \quad (12)$$

Other work has stated that adding gain to a meta-material system compensates for losses by creating transparency and enhancing field amplification. [17] Additionally, theoretical models have proposed that alternating stacks of silver and amplifying dielectric medium compensate for the losses in the superlens and create better resolution performance. [18] We contend that adding

gain to the entire superlens does not enhance the magnitude of the H-field or field intensity unless the gain compensates for losses exactly, which is very difficult to achieve experimentally. Gain merely adds a phase of  $\pi$  to the loss parameter  $\phi$ . Fig. 3 shows the absolute value of the transfer in and out functions do not change for gain parameters. The transfer function symmetry from absorption and gain parameters leads us to conclude that the resolving capabilities of the superlens system is the same for equal absorption and gain conditions.

Our superlens simulations show that surface plasmon polariton (SPP) excitation occurs at both lens interfaces in the symmetric configuration ( $2a = b$ ) when the size of the system is sufficiently small. In this regime the evanescent spectrum is the primary field component in the signal as seen by Fig. 2. Amplification of evanescent waves at the lens boundaries allows this imaging system to resolve subwavelength features by recovering field components that are commonly lost due to exponential decay.

At the boundary of the diffraction limited region, when the focal distance is equal to the wavelength of the source, the field maximums still occur at both interfaces but the propagating region of the spectrum begins to increase as seen by Fig. 2. For focal distances beyond one wavelength, field intensity maximums at both interfaces decrease as the propagating spectrum components provide the majority of the wave behavior. Note that the maximums occur in the center of the lens and at the image location for the symmetric configuration when the lens is in the far-field.

We derive the resolution limit  $\Delta$  of the system by describing the spatial size of a wave packet at the image location ( $x = 0; z = 2b$ ). [16] If we define  $\delta$  as the spectral width, or range of  $k_x$  values, then there is some  $k_x$  value equal to  $\delta/2$  where the wavevector spectrum equals  $w/2$ .

$$\frac{w}{2} = 4 \frac{\sin(w\delta/2)}{\delta} \quad (13)$$

Now we make two substitutions to relate the spatial wave packet size to the spectral width using the *optical uncertainty principle*. First set  $w\delta = x$ , and then set  $4\pi\xi = x$ , to obtain the resolution in terms of spectral width. For our single slit geometry the variable  $\xi \approx 0.6$ .

$$\Delta \cdot \delta = 4\pi\xi \quad (14)$$

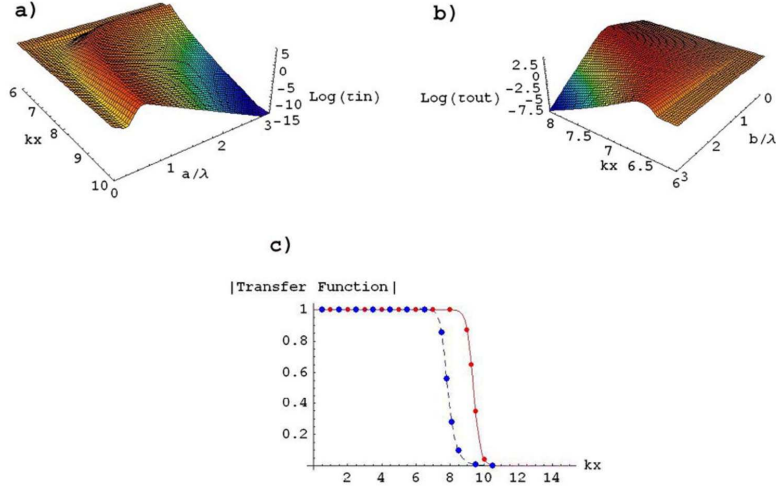


Figure 3: a) Transfer-in function at the front interface plotted as a function of focal distance  $a\lambda$  and  $k_x$  with  $\epsilon'' = \mu'' = 10^{-3}$ . b) Transfer-out function at the back interface plotted as a function of lens thickness  $b\lambda$  and  $k_x$  with  $\epsilon'' = \mu'' = 10^{-3}$ . c) The solid red line is the absolute value of the transfer-out function at the image location with absorption given by  $\epsilon'' = \mu'' = 10^{-6}$ . The red dots are the absolute value of the transfer-out function at the image location with gain given by  $\epsilon'' = \mu'' = -10^{-6}$ . The dashed blue line is the absolute value of the transfer-in function at the first focus with absorption given by  $\epsilon'' = \mu'' = 10^{-4}$ . The blue dots represent the absolute value of the transfer-in function with gain given by  $\epsilon'' = \mu'' = -10^{-4}$ . The focal distance for the third graph is  $1.0\lambda$ , the lens thickness is  $2.0\lambda$ , and the slit width is  $0.1\lambda$ .

The previous equation is informative, but a more useful resolution equation depending on lens thickness and system absorption can be derived by studying the transfer out function shown in Eq(11). At some critical wavevector value  $k_x^0 = \delta/2$ ,  $\tau_{out} = 1/2$ , so the resolution can be found by solving the following transcendental equation.

$$\frac{2\pi b}{\lambda} = -\frac{\ln \frac{1}{2} \left[ \epsilon'' + \frac{\epsilon'' + \mu''}{2\chi^2} \right]}{\chi} \quad (15)$$

In the above equation  $\chi = \sqrt{k_x^0 c^2 / \omega^2 - 1} = \sqrt{\xi^2 \lambda^2 / \Delta^2 - 1}$ . By assuming that we are in the near-field regime where subwavelength resolution,  $\Delta \ll \lambda$ , is possible we can further reduce Eq(15) using the property  $\chi \approx \xi\lambda/\Delta$  to write an expression for the resolution of the symmetric superlens configuration.

$$\Delta \approx -\frac{2\pi b}{\ln(\epsilon''/2)} \quad (16)$$

As stated previously, the lens thickness must be at least as large as the focal distance. When

the lens thickness is exactly equal to the focal distance ( $a = b$ ), the system is in the *optimal* configuration. In the optimal configuration the image is located on the back interface, so information can be easily gathered through the detector placement on the lens boundary. In addition to the detection strengths, the optimal configuration provides the highest amount of subwavelength field resolution. An equation describing the resolution of the optimal configuration is shown below.

$$\Delta \approx -\frac{2\pi a}{\ln(\epsilon''/2)} \quad (17)$$

### Transition to Diffraction Limited Imaging

The previous section described the near-field resolution capabilities of the planar NIM lens, but what defines the near-field regime for this system? As the lens thickness is increased the image moves further away from the source, therefore lens thickness is a general variable that confines the imaging properties of the lens. System absorption is the other primary parameter we chose to model. The primary mechanism for subwavelength resolution is the amplification and recovery of evanescent field components at the image location. To understand the transition to diffraction limited imaging behavior we calculate the evanescent and propagating fields from a point source to compare their magnitudes as the lens thickness and system absorption vary. Our point source term is represented by the Green function,  $G_R = (i/4)hH_0^{(1)}(\rho k_0)$ , where  $\rho = \sqrt{x^2 + z^2}$ , and the Hankel function  $H_0^1 = J_0 + iN_0$ . [19, 20] Where our work differs is in the use of an *exact* transfer function to calculate field components. To calculate field components at the image location ( $z = 2b$ ) we must integrate exact transfer out equations multiplied by delta source terms. Below is the exact transfer out function from which the previous series solution shown in Eq(11) was derived.

$$\tau_{exact} = -\frac{4\epsilon k_1 k_2 \exp(i(k_1 + k_2)b)}{\exp(ik_2 b)(k_2 - \epsilon k_1) - (\epsilon k_1 + k_2)^2} \quad (18)$$

The subscripts on the k values refer to the specific system region, where 2 is inside the lens and 1 is outside the lens. The general propagating wavevector expression is written

$$k_i = \sqrt{\epsilon_i \mu_i \frac{\omega^2}{c^2} - k_x^2} \quad (19)$$

To find the field resulting from the propagating and evanescent spectra solving the integrals below is required. Note that the  $1/k_1$  term in the integral was derived using fourier analysis of the Green function source function.

$$\vec{H}_p = \int_{-\omega/c}^{\omega/c} \frac{\tau_{exact}}{k_1} dk_x \quad (20)$$

$$\vec{H}_{ev} = \int_{|k_x| > \omega/c}^{\infty} \frac{\tau_{exact}}{k_1} dk_x \quad (21)$$

In the limit where  $kb \gg 1$  the propagating field component is a constant of order 1. As the lens thickness increases the exact transfer out function can be simplified by neglecting the exponential term in the denominator. The integrand in the evanescent field equation decays exponentially for  $k_x > \omega/c$ . By taking a power series about  $\epsilon'' = \mu'' = 0$  the propagating wavevector to first order takes the form

$$k_2 \cong k_1 - \frac{1}{2} \frac{i(\epsilon'' + \mu'') \omega^2}{k_1 c^2} \quad (22)$$

By using the  $k_2$  definition above with the reduced exact transfer out equation we are able to provide a very useful analytical expression for the evanescent field at the image location. If we define  $\alpha = \sqrt{\frac{1}{2}(\epsilon'' + \mu'')}$  the evanescent field at the image location is described by the expression below.

$$\vec{H}_{ev} \cong \frac{4c^2}{\omega^2 b^2 \alpha} \exp\left(-\frac{\omega}{c} \alpha b\right) \frac{\cos\left(\frac{\omega}{c}\right) \alpha b - i \sin\left(\frac{\omega}{c}\right)}{(1 - i)} \quad (23)$$

The criteria used to describe the transition from subwavelength to diffraction-limited imaging is the ratio  $P = \frac{|H_{ev}|}{|H_p|}$ . When  $P \ll 1$  the system is in the diffraction-limited far-field regime, and when  $P \gg 1$  the imaging system can have superresolution. A general variable containing information about the total system absorption and lens length is defined as a fundamental parameter of  $P$ . The variable  $k_0$  is defined to be  $\omega/c$ .

$$S = k_0 b \sqrt{\text{Im} \left( \frac{\epsilon + \mu}{2} \right)} = k_0 b \sqrt{\delta} \quad (24)$$

When  $S \ll 1$  the planar lens ratio is defined as

$$P(S) = \frac{1}{k_0 b} \frac{4(i \sin(S) - \cos(S)) \exp(-S)}{S(i-1)} \ll 1 \quad (25)$$

When  $S \gg 1$  the planar lens ratio is defined as

$$P(S) \simeq \frac{2}{i\pi} \ln \left[ -\frac{2 \ln(\delta/4)}{k_0 b} \right] \quad (26)$$

Our transition analysis provided us with data that describes the transition from near-field to diffraction limited far-field lens behavior as a function of lens thickness and system absorption. In addition to describing fields from the propagating and evanescent spectra, we used numerical integration and root finding computational techniques to find lens thickness and absorption data points corresponding to image location evanescent field magnitudes that are equal to some fraction of the propagating field.

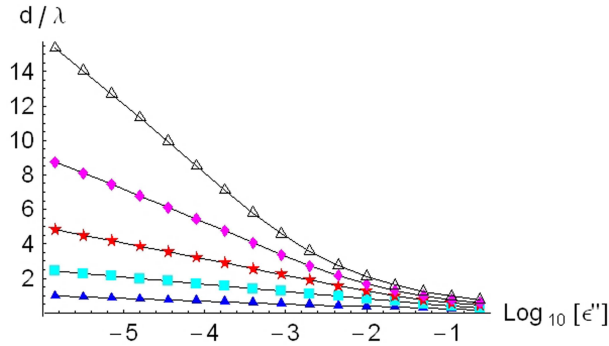


Figure 4: Normalized transition lens thickness and absorption data for the Planar NIM lens with a point source. Absorption values range from  $10^{-6} < \epsilon'' < 0.25$ . Data was found by setting  $H_{ev} = q \cdot H_p$ . Blue triangle data points correspond to  $q = 1$ . Light blue solid boxed data points correspond to  $q = 1/2$ . Red stars correspond to  $q = 1/4$ . Pink diamond data points correspond to  $q = 1/8$ . Black hollow triangles correspond to  $q = 1/16$ .

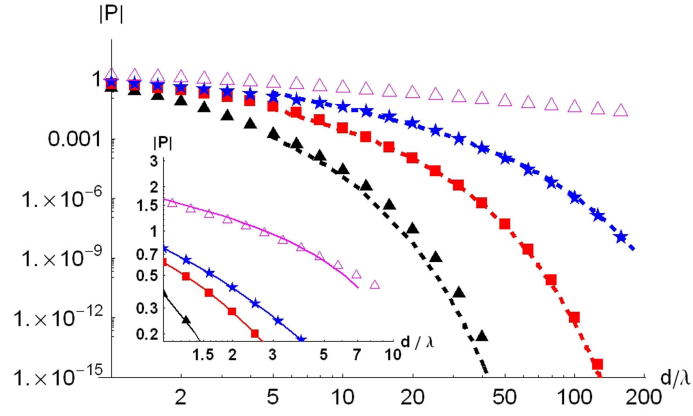


Figure 5: Functional behavior of the ratio  $|P|$  for  $\delta = 10^{-2}$  (solid triangles),  $\delta = 10^{-3}$  (boxes),  $\delta = 10^{-4}$  (stars), and  $\delta = 10^{-18}$  (hollow triangles). Symbols are results of numerical integration while dashed and dotted lines represent approximate equations shown in Eq(26, 27).

### Far-Field Diffraction Limited Imaging Properties of the Superlens

To discuss the resolution limitations of the superlens in the far-field, we consider a point cylindrical wave source located at  $x = 0, z = 0$ . Source waves are projected onto the front lens interface, with coordinates  $x = x_1$  and  $z = a$ , and then collected again at the first focus when  $z = 2a$ . It has been shown that the smearing of the foci at the first and second focal points are equal, accordingly, only the first will be considered in this work. [19, 20] The field inside of the lens region is given by the Fresnel integral

$$H(x, z) = \int_{-\infty}^{\infty} \frac{a}{(a^2 + x_1^2)^{\frac{1}{2}}} \frac{\text{Exp} \left[ i \cdot k (a^2 + x_1^2)^{\frac{1}{2}} \right]}{(a^2 + x_1^2)^{\frac{1}{4}}} \frac{\text{Exp} \left[ -i \cdot k ((z - a)^2 + (x_1 - x)^2)^{\frac{1}{2}} \right]}{((z - a)^2 + (x_1 - x)^2)^{\frac{1}{4}}} dx_1 \quad (27)$$

The first term of Eq (27) describes the propagating  $k$  component of the cylindrical source given some  $k_x$  value, the second term represents the projection of the cylindrical source waves onto the lens interface, and the third term represents individual source waves at  $z = a$  moving inside the lens to the first focus. By making a substitution  $\eta = z - 2a$ , and taking the series of the above equation close to the first focal point we get the expression

$$H(x, z) = \int_{-\infty}^{\infty} \frac{\text{Exp} \left[ i \cdot k \frac{(x_1 x - a \eta)}{(a^2 + x_1^2)^{\frac{1}{2}}} \right]}{a^2 + x_1^2} dx_1 \quad (28)$$

By substituting  $x_1 = a \tan u$  we obtain the field in an integral form that can be calculated numerically.

$$H(x, z) = \frac{1}{a} \int_{-\frac{\pi}{2}}^{\frac{\pi}{2}} \text{Exp}[i \cdot k(x \sin u - \eta \cos u)] du \quad (29)$$

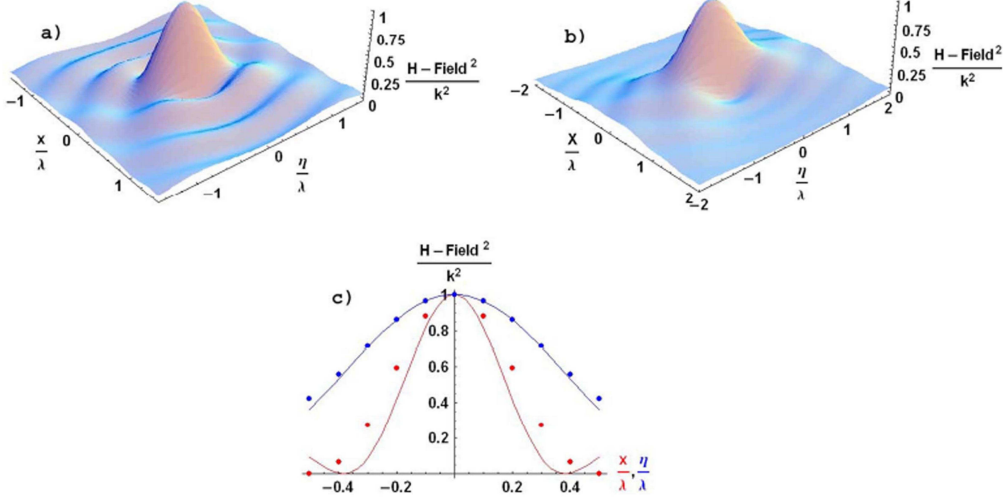


Figure 6: a) Numerical plot of H-Field intensity at the first focus  $z = 2a$  using Eq (29). b) Numerical plot of H-Field intensity at the first focus using Eq (8) with 100  $dk_x$  iterations. c) Two dimensional  $x$  and  $z$  cross-sections around the first focus. Dotted data points are from the Eq (8) calculation. Notice the the field is not confined symmetrically in the  $x$  and  $z$  directions.

Although the full field calculation must be solved numerically, the  $x$  cross section ( $\eta = 0$ ) and the  $z$  cross section ( $x = 0$ ) can be solved for analytically. First we will start by defining a new angle with the properties  $\tan \psi = \frac{\eta}{x}$  and then turn Eq (29) into

$$H(x, z) = \frac{1}{a} \int_{-\frac{\pi}{2}}^{\frac{\pi}{2}} \text{Exp}[i \cdot k\sqrt{x^2 + \eta^2} \sin(u - \psi)] du \quad (30)$$

As  $\eta \rightarrow 0$ ,  $\psi \rightarrow 0$ , the field expression for the  $x$  cross section becomes  $\frac{\pi}{a} J(0, kx)$ . As  $x \rightarrow 0$ ,  $\psi \rightarrow \frac{\pi}{2}$ , the field expression for the  $z$  cross section becomes  $\frac{\pi}{a} (J(0, k\eta) - iH(0, k\eta))$ , where  $J$  is a Bessell function and  $H$  is a Struve function. The imaginary part of the field expression for the  $z$  cross section makes the field intensity plot anti-symmetric. The resolution of the far-field system based on full width half maximum H-field intensity measurements is limited because the image at the first focus is confined anti-symmetrically. We would also like to note that the H-Field at

the first focus is confined to a region smaller than  $\lambda/2$  in the far-field measurements, but we do not consider this to be subwavelength imaging.

## Conclusions

Subwavelength resolution is achieved by the planar NIM lens in the near-field regime due to amplification and recovery of evanescent field components. Single slit source analysis shows the formation of Surface Plasmon Polaritons at both lens interfaces, which could give rise to interesting new optical devices. By using a point source and Green's function analysis combined with exact transfer functions for the system we were able to classify the transition to diffraction limited imaging behavior as a function of system absorption and size. Far-field analysis was performed by calculating fields using a Fresnel integral to show asymmetric field confinement and diffraction limited resolution.

## Acknowledgements

I would like to thank Viktor Podolskiy and his students, Alexander Govyadinov, Justin Elser, Robyn Wangberg, and Ken Lett sincerely for all of our research collaborations at Oregon State University. Both Graeme W. Milton and Alexei L. Efros from the University of Utah have collaborated with us on multiple projects, and we thank them for communicating their tremendous insight. We would like to thank Robert Burton for helpful mathematical technique discussions and Heather L. Kuhta for editing support. The work has been partially supported by GRF(OSU) and PRF(ACS).

## References

- [1] V.G. Veselago, *The Electrodynamics of Substances with Simultaneous  $\epsilon$  and  $\mu$* , Sov. Phys. Usp. **10**, 509 (1968)
- [2] Zhaowei Liu, et al., *Far-Field Optical Hyperlens Magnifying Sub-Diffraction-Limited Objects*, Science **315**, 1686 (2007)
- [3] Igor I. Smolyaninov, et al., *Magnifying Superlens in the Visible Frequency Range*, Science **315**, 1699 (2007)
- [4] Mehmet Fatih Yanik, Shanhui Fan, Marin Soljagic, J.D. Joannopoulos, *All-optical transistor action with bistable switching in a photonic crystal with cross-waveguide geometry.*, Opt. Lett. **28**, 2506 (2003)

- [5] J.B. Pendry, *Negative Refraction Makes a Perfect Lens*, Phys. Rev. Lett. **84**, 3966 (2000)
- [6] Nicholas Fang, Hyesog Lee, Cheng Sun, Xiang Zhang, Science **308**, 534 (2005)
- [7] R.A. Shelby, D.R. Smith, S. Schultz, Science **292**, 77 (2001)
- [8] Stefan Linden, Christian Enkrich, Martin Wegener, Jiangfeng Zhou, Thomas Koschny, Costas M. Soukoulis, *Magnetic Response of Metamaterials at 100 Terahertz*, Science **306** 1351 (2004)
- [9] J.B. Pendry, A.J. Holden, D.J. Robbins, W.J. Stewart, IEEE Trans. Microwave Theory Tech. **47**, 2075 (1999)
- [10] Wenshan Cai, Dentcho A. Genov, Vladimir M. Shalaev, PHYSICAL REVIEW B. **72**, 193101 (2005)
- [11] V.A. Podolskiy, E.E. Narimanov, Opt. Lett. **30**, 75 (2005)
- [12] J.W. Goodman, *Introduction to Fourier Optics* (Roberts and Company, Greenwood Village, CO, 2004); M. Born, E. Wolf, *Principles of Optics*, 7th ed. (Cambridge University Press, New York, 2003)
- [13] D.R. Smith, D. Schurig, M. Rosenbluth, S. Schultz, S.A Ramakrishna, J.B. Pendry, Appl. Phys. Lett. **82** 1506 (2003)
- [14] K. J. Webb, M. Yang, D.W. Ward, K.A. Nelson, Phys. Rev. B. **70** 035602(R) (2004); M.-C. Yang, K.J. Webb, Opt. Lett. (2005)
- [15] Graeme W. Milton, Nicholae-Alexandru P. Nicorovici, *On the cloaking effects associated with anomalous localized resonance*, Proc. Roy. Soc. A, doi:10.1098,rspa.2006.1715
- [16] Viktor A. Podolskiy, Nicholas A. Kuhta, Graeme W. Milton, App. Phys. Lett. **87**, 231113 (2005)
- [17] Alexander K. Popov, Vladimir M. Shalaev, *Compensating losses in negative-index metamaterials by optical parametric amplification*, Opt. Lett. **31**, 2169 (2006)
- [18] S. Anantha Ramakrishna, J.B. Pendry, *Removal of absorption and increase in resolution in a near-field lens via optical gain*, PHYSICAL REVIEW B **67**, 201101(R) (2003)
- [19] A.L. Pokrovsky, A.L. Efros, *Diffraction theory and focusing of light by left-handed materials*, arXiv:cond-mat/0207534 v1 **22** Jul (2002)
- [20] Chengyu Li, J.M. Holt, A.L. Efros *Far-field Imaging by the Veselago lens made of a photonic crystal*, J. Opt. Soc. Am. B, Vol. **23**, No. 3, March (2006)